



RESEARCH PAPER

Re-writing Oral Pharmacokinetics Using Physiologically Based Finite Time Pharmacokinetic (PBFTPK) Models

Pavlos Chryssafidis^{1,2} · Athanasios A. Tsekouras^{1,3} · Panos Macheras^{1,2}

Received: 23 January 2022 / Accepted: 9 March 2022 / Published online: 4 April 2022
© The Author(s), under exclusive licence to Springer Science+Business Media, LLC, part of Springer Nature 2022

Abstract

Purpose To develop physiologically based finite time pharmacokinetic (PBFTPK) models for the analysis of oral pharmacokinetic data.

Methods The models are based on the passive drug diffusion mechanism under the sink conditions principle. Up to three drug successive input functions of constant rate operating for a total time τ are considered. Differential equations were written for all these models assuming linear one- or two-compartment-model disposition. The differential equations were solved and functions describing the concentration of drug as a function of time for the central and the peripheral compartment were derived. The equations were used to generate simulated data and they were also fitted to a variety of experimental literature oral pharmacokinetic data.

Results The simulated curves resemble real life data. The end of the absorption processes τ is either equal to t_{\max} or longer than t_{\max} at the descending portion of the concentration time curve. Literature oral pharmacokinetic data of paracetamol, ibuprofen, almotriptan, cyclosporine (a total of four sets of data), and niraparib were analyzed using the PBFTPK models. Estimates for τ corresponding to a single or two or three different in magnitude input rates were derived along with the other model parameters for all data analyzed.

Conclusions The PBFTPK models are a powerful tool for the analysis of oral pharmacokinetic data since they rely on the physiologically sound concept of finite absorption time.

KEY WORDS almotriptan · cyclosporine · finite absorption time · ibuprofen · niraparib · oral drug absorption · oral pharmacokinetics · paracetamol · physiologically based finite time pharmacokinetic models

Abbreviations

FAT	Finite absorption time
PBFTPK	Physiologically based finite time pharmacokinetic
PBPK	Physiologically based pharmacokinetic

✉ Athanasios A. Tsekouras
thanost@chem.uoa.gr

✉ Panos Macheras
macheras@pharm.uoa.gr

Pavlos Chryssafidis
pxrissafidis@gmail.com

¹ PharmaInformatics Unit, Research Center ATHENA, Athens, Greece

² Faculty of Pharmacy, Laboratory of Biopharmaceutics Pharmacokinetics, National and Kapodistrian University of Athens, Athens, Greece

³ Present Address: Department of Chemistry, Laboratory of Physical Chemistry, National and Kapodistrian University of Athens, Athens, Greece

Introduction

The term pharmacokinetics was first introduced by F. H. Dost in 1953 in his text, *Der Blutspiegel. Kinetik der Konzentrationsabläufe in der Kreislaufflüssigkeit* (1). Dost adopted the Bateman equation to describe the concentration of drug in plasma, $C(t)$, assuming first-order absorption (input) and first-order elimination

$$C(t) = \frac{FDk_a}{V_d(k_a - k_{el})} (e^{-k_{el}t} - e^{-k_a t}) \quad (1)$$

where F is the bioavailable fraction of dose D , V_d is the volume of distribution and k_a , k_{el} are the absorption and elimination first-order rate constants, respectively. This equation implies that absorption and elimination run concurrently for infinite time.

The finite time of oral drug absorption concept has been sporadically used (2–5) in the context of classical first-order

absorption kinetics, i.e., Eq. 1 applies only for a specific time period. Due to the fact that the blood flow in the portal vein has a velocity of 20–40 cm/s (6), sink conditions prevail for the drug transfer from the gastrointestinal lumen to the blood stream. This led to the development of physiologically based finite time pharmacokinetic (PBFTPK) models and the corollary zero-order drug input (7). The basic features of the PBFTPK models are the finite termination times lower than 5 and 30 h, for drug absorption in the small intestines and colon, respectively (7, 8). In parallel, multiple-successive constant drug input rates were also considered (7) in line with the varying character of drug absorption because of the potential dissolution/precipitation/re-dissolution and/or regional drug permeability in jejunum, ileum, colon of the gastrointestinal tract.

In this work, we formally define the basic PBFTPK modes, which interpret oral drug kinetic data in terms of the finite absorption time (FAT) concept. To this end, we also

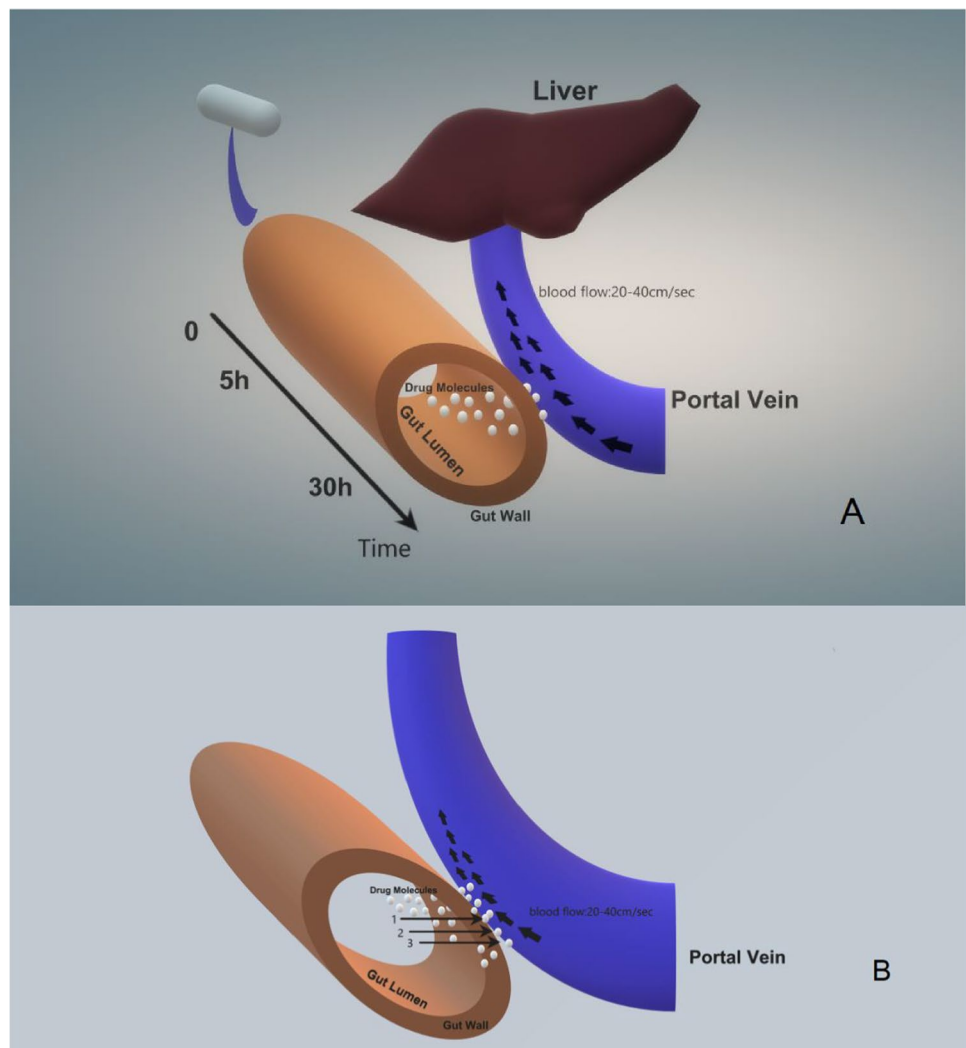
carry simulations and apply the PBFTPK modes for fitting purposes using the PBFTPK software developed.

Theory

According to the fundamental model developed in (7), drugs are absorbed passively under sink conditions for physiological reasons (6), Fig. 1A. Drug absorption under sink conditions has been used and is still used extensively and successfully in physiologically based pharmacokinetic (PBPK) modeling (9, 10). Due to the anatomical-physiological characteristics of the gastrointestinal tract, drugs with different biopharmaceutical properties, e.g., solubility, permeability, ionization, can exhibit one or two or three successive constant input rates, Fig. 1B.

For drugs following linear disposition kinetics, we coin the term p -PBFTPK- m , where p is the number of the successive input rates 1, 2, 3 and m takes the values 1 or 2 denoting

Fig. 1 (A) Schematic of the passive transfer of dissolved drug molecules (white spheres) from the gut lumen to portal vein. The blood flow in the portal vein, 20–40 cm/s (6) ensures sink conditions for the passive drug transfer due to its continuous removal from the portal vein to liver. The physiological time limits 5 and 30 h for drug absorption from the small intestines and colon (7, 8), respectively are shown on the time axis. (B) Enlargement of the region gut wall-portal vein for the drug transfer; the arrows indicate up to three successive constant input rates for the dissolved drug molecules (white spheres) passive transfer under sink conditions.



the disposition characteristics of drug, namely, one- or two-compartment model, respectively. For the metabolized drugs following non-linear Michaelis–Menten disposition kinetics we coin the term p -PBFTP K - m (MM). A schematic representation of models exhibiting linear or non-linear disposition kinetics is shown in Fig. 2.

The differential equations for the linear models, p -PBFTP K - m are listed in Table I. The corresponding equations for drug's concentration change as a function of time in the central compartment, $C(t)$, and in the peripheral compartment, $P(t)$, for these models are listed in Table II and III. It should be noted that the ratio of the distribution volumes of the central and the peripheral compartment is not

included explicitly in the following expressions. This does not affect any calculations or conclusions because there are no data on the actual drug concentration in the peripheral compartment.

Materials and Methods

Simulations

The analytic model equations of Tables II and III were used to generate concentration – time profiles assigning various values to the model parameters.

Fig. 2 Schematic representation of one compartment (A) and two compartment (B) p -PBFTP K - m models. In all cases the horizontal arrows at the left-hand side of the central compartment denote the number of successive constant drug input rates, not necessarily of the same drug amount or duration; k_{el} is the elimination rate constant, k_{10} is the elimination rate constant of the central compartment of the two compartment model drugs; k_{12} and k_{21} are the disposition micro-constants for the transfer of drug from the central to peripheral compartment and vice versa, respectively; V_{max} and K_M correspond to the maximum biotransformation rate and the constant of the Michaelis–Menten kinetics.

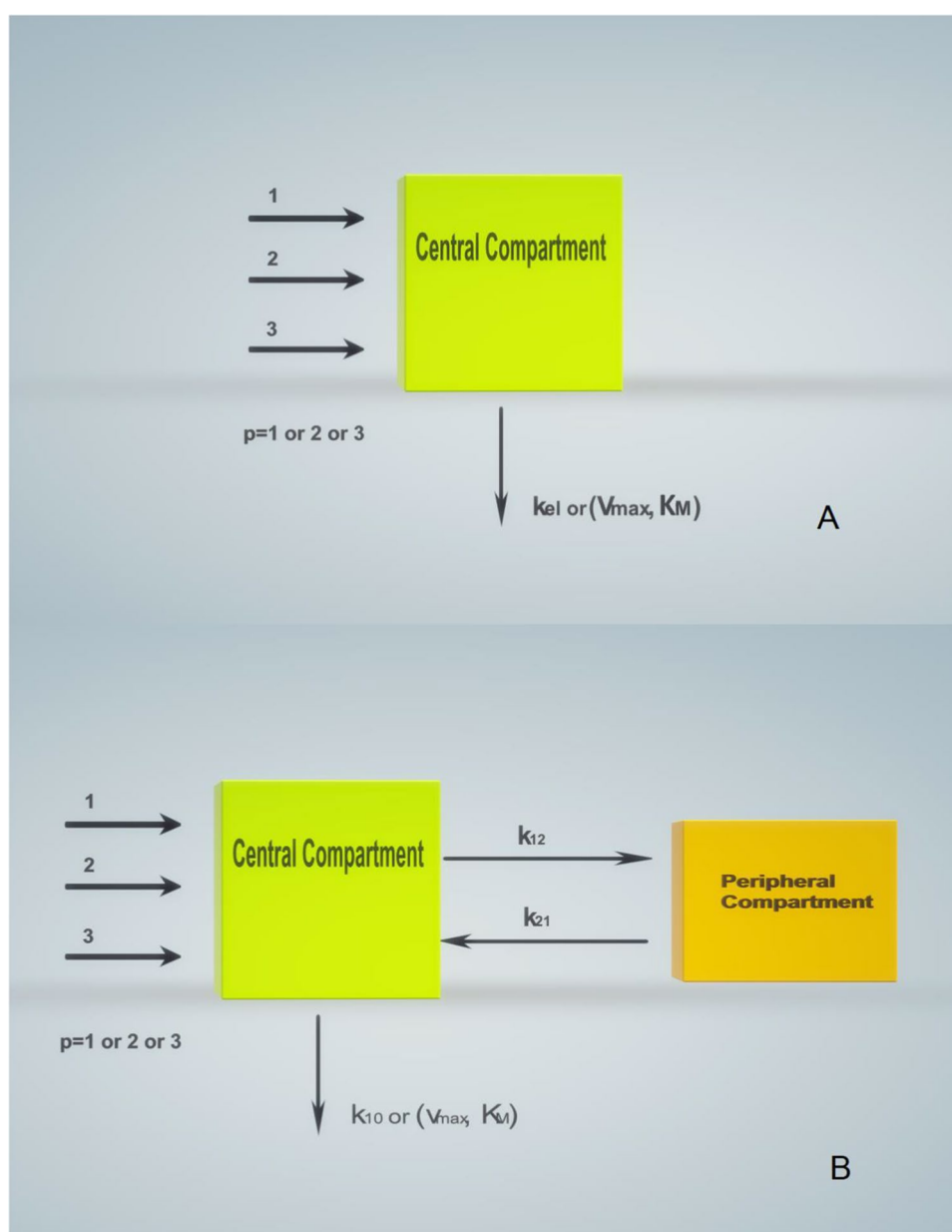


Table I Differential Equations or Linear Models *p*-PBFTPK-*m*

<i>p</i>	<i>m</i>	Kinetic (differential) equations	$t_1 < t \leq t_2$		Eq
1	1	$\frac{dC}{dt} = \frac{FD}{\tau V_d} - k_{el}C$	0	τ	2
		$\frac{dC}{dt} = -k_{el}C$	τ	∞	3
2	1	$\frac{dC}{dt} = \frac{F_1D}{\tau_1 V_d} - k_{el}C$	0	τ_1	4
		$\frac{dC}{dt} = \frac{F_2D}{\tau_2 V_d} - k_{el}C$	τ_1	$\tau_1 + \tau_2$	5
		$\frac{dC}{dt} = -k_{el}C$	$\tau_1 + \tau_2$	∞	6
3	1	$\frac{dC}{dt} = \frac{F_1D}{\tau_1 V_d} - k_{el}C$	0	τ_1	7
		$\frac{dC}{dt} = \frac{F_2D}{\tau_2 V_d} - k_{el}C$	τ_1	$\tau_1 + \tau_2$	8
		$\frac{dC}{dt} = \frac{F_3D}{\tau_3 V_d} - k_{el}C$	$\tau_1 + \tau_2$	$\tau_1 + \tau_2 + \tau_3$	9
		$\frac{dC}{dt} = -k_{el}C$	$\tau_1 + \tau_2 + \tau_3$	∞	10
1	2	$\frac{dC}{dt} = \frac{FD}{\tau V_d} - k_{12}C - k_{10}C + k_{21}P$	0	τ	11
		$\frac{dP}{dt} = k_{12}C - k_{21}P$			12
		$\frac{dC}{dt} = -k_{12}C - k_{10}C + k_{21}P$	τ	∞	13
		$\frac{dP}{dt} = k_{12}C - k_{21}P$			14
2	2	$\frac{dC}{dt} = \frac{F_1D}{\tau_1 V_d} - k_{12}C - k_{10}C + k_{21}P$	0	τ_1	15
		$\frac{dP}{dt} = k_{12}C - k_{21}P$			16
		$\frac{dC}{dt} = \frac{F_2D}{\tau_2 V_d} - k_{12}C - k_{10}C + k_{21}P$	τ_1	$\tau_1 + \tau_2$	17
		$\frac{dP}{dt} = k_{12}C - k_{21}P$			18
		$\frac{dC}{dt} = -k_{12}C - k_{10}C + k_{21}P$	$\tau_1 + \tau_2$	∞	19
		$\frac{dP}{dt} = k_{12}C - k_{21}P$			20
3	2	$\frac{dC}{dt} = \frac{F_1D}{\tau_1 V_d} - k_{12}C - k_{10}C + k_{21}P$	0	τ_1	21
		$\frac{dP}{dt} = k_{12}C - k_{21}P$			22
		$\frac{dC}{dt} = \frac{F_2D}{\tau_2 V_d} - k_{12}C - k_{10}C + k_{21}P$	τ_1	$\tau_1 + \tau_2$	23
		$\frac{dP}{dt} = k_{12}C - k_{21}P$			24
		$\frac{dC}{dt} = \frac{F_3D}{\tau_3 V_d} - k_{12}C - k_{10}C + k_{21}P$	$\tau_1 + \tau_2$	$\tau_1 + \tau_2 + \tau_3$	25
		$\frac{dP}{dt} = k_{12}C - k_{21}P$			26
		$\frac{dC}{dt} = -k_{12}C - k_{10}C + k_{21}P$	$\tau_1 + \tau_2 + \tau_3$	∞	27
		$\frac{dP}{dt} = k_{12}C - k_{21}P$			28

Model Fittings

The model equations were fitted to experimental data obtained from the literature. The PBFTPK software used in all model fittings relies on user defined functions in Igor programming environment. In this implementation we adapted its versatile built-in least squares algorithm which allows, among other features, restrictions to parameter values, the use of statistical weights and data sub-sets, calculation of parameter covariance matrix, and easy graphical representation of results. Due to the complex form of the model equations and the convoluted shape of the resulting x^2 hypersurface in parameter space with numerous local minima, the determination of initial trial parameter values was crucial and required their manual adjustments.

Results

Simulations

Figures 3 and 4 show simulated concentration–time curves generated from the model equations for one- and two-compartment model drugs, respectively. Both Figures demonstrate the resemblance of the simulated curves with real life data reported in the literature. When a single input rate is applied (Fig. 3A, Fig. 4A), the simulated data exhibit a patent change of drug concentration $C(\tau)$ at the end of the duration of the absorption process at time τ , (marked with the symbol \blacktriangle), which also corresponds to the maximum drug concentration, C_{max} , observed in plasma. For the simulated data with multiple input rates, the values of $C(\tau)$ can be either equal to C_{max} (Figs. 3B, D, 4D) or smaller (Fig. 3C, 4B, C), i.e., the termination of the absorption phase is observed at the descending limb of the curve. The simulated results for the $P(t)$ curves show the shape similarity of

Table II Solutions to Linear Models *p*-PBFTPK-1

<i>p</i>	<i>m</i>	$C(t)$	$t_1 < t \leq t_2$		Eq
1	1	$\frac{FD}{\tau V_d k_{el}} (1 - e^{-k_{el}t})$	0	τ	29
		$C(\tau)e^{-k_{el}(t-\tau)}$	τ	∞	30
2	1	$\frac{F_1D}{\tau_1 V_d k_{el}} (1 - e^{-k_{el}t})$	0	τ_1	31
		$C(\tau_1)e^{-k_{el}(t-\tau_1)} + \frac{F_2D}{\tau_2 V_d k_{el}} (1 - e^{-k_{el}(t-\tau_1)})$	τ_1	$\tau_1 + \tau_2$	32
		$C(\tau_1 + \tau_2)e^{-k_{el}(t-\tau_1-\tau_2)}$	$\tau_1 + \tau_2$	∞	33
3	1	$\frac{F_1D}{\tau_1 V_d k_{el}} (1 - e^{-k_{el}t})$	0	τ_1	34
		$C(\tau_1)e^{-k_{el}(t-\tau_1)} + \frac{F_2D}{\tau_2 V_d k_{el}} (1 - e^{-k_{el}(t-\tau_1)})$	τ_1	$\tau_1 + \tau_2$	35
		$C(\tau_1 + \tau_2)e^{-k_{el}(t-\tau_1-\tau_2)} + \frac{F_3D}{\tau_3 V_d k_{el}} (1 - e^{-k_{el}(t-\tau_1-\tau_2)})$	$\tau_1 + \tau_2$	$\tau_1 + \tau_2 + \tau_3$	36
		$C(\tau_1 + \tau_2 + \tau_3)e^{-k_{el}(t-\tau_1-\tau_2-\tau_3)}$	$\tau_1 + \tau_2 + \tau_3$	∞	37

Table III Solutions to Linear Models p -PBFTP K -2[†]

p	m	$C(t), P(t)$	$t_1 < t_2 \leq t_3$	Eq
1	2	$C(t) = \frac{FD}{\tau V_d} \left(\frac{(k_{21}-\alpha)(1-e^{-\alpha t})}{\alpha(\beta-\alpha)} + \frac{(k_{21}-\beta)(1-e^{-\beta t})}{\beta(\alpha-\beta)} \right)$ $P(t) = \frac{FDk_{12}}{(\beta-\alpha)\tau V_d} \left[\frac{1}{\alpha} (1-e^{-\alpha t}) - \frac{1}{\beta} (1-e^{-\beta t}) \right]$ $C(t) = \frac{FD}{\tau V_d} \frac{(k_{21}-\alpha)(1-e^{-\alpha t})}{\alpha(\beta-\alpha)} + \frac{FD}{\tau V_d} \frac{(k_{21}-\beta)(1-e^{-\beta t})}{\beta(\alpha-\beta)} e^{-\beta(t-\tau)}$	0	38
			τ	39
			∞	40
				41
2	2	$P(t) = \frac{k_{12}}{\beta-\alpha} \left((C(\tau) + \frac{k_{21}P(\tau)}{k_{21}-\alpha}) e^{-\alpha(t-\tau)} - (C(\tau) + \frac{k_{21}P(\tau)}{k_{21}-\beta}) e^{-\beta(t-\tau)} \right)$ $C(t) = \frac{F_1 D k_{12}}{\tau_1 V_d} \left[\frac{1}{\alpha} (1-e^{-\alpha t}) + \frac{k_{21}-\beta}{\beta(\alpha-\beta)} (1-e^{-\beta t}) \right]$	0	42
			τ_1	43
				44
			$\tau_1 + \tau_2$	45
			∞	46
				47
			τ_1	48
				49
			$\tau_1 + \tau_2$	50
				51
			$\tau_1 + \tau_2$	52
				53
			∞	54
			$\tau_1 + \tau_2 + \tau_3$	55
			∞	56

[†] In all cases, $\alpha + \beta = k_{12} + k_{21} + k_{10}$ and $\alpha\beta = k_{21}k_{10}$

Fig. 3 Simulated curves for one compartment model drugs ($m=1$) following linear disposition kinetics with $p=1$ (Eqs. 29–30, panel (A)), $p=2$ (Eqs. 31–33, panel (B)), $p=3$ (Eqs. 34–37, panels (C) and (D)). Model parameter values are shown in each panel. The symbol \blacktriangle denotes termination of all absorption stages.

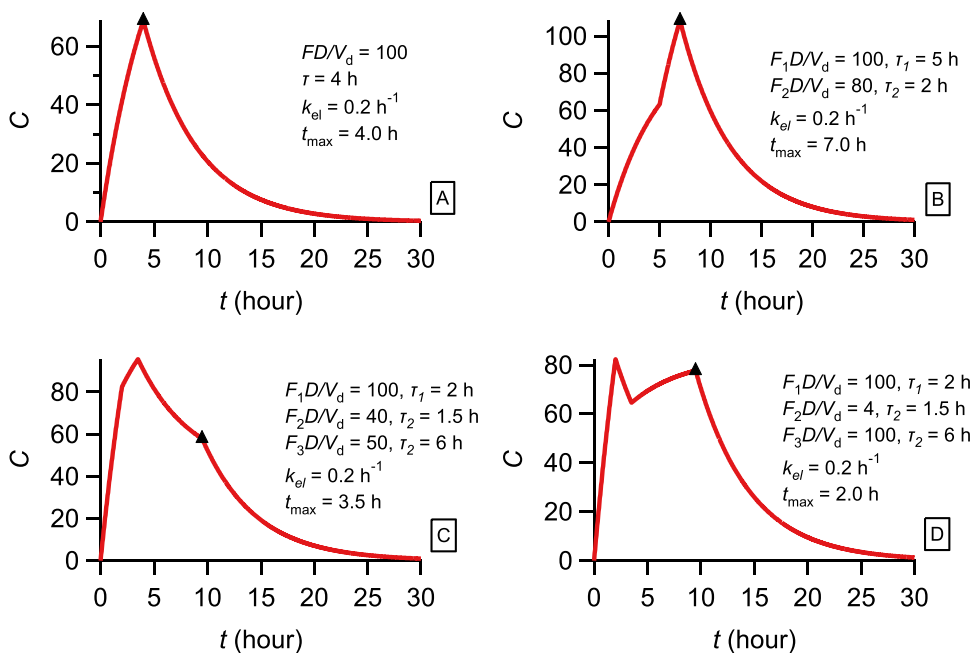


Fig. 4 Simulated curves for two compartment model drugs ($m=2$) following linear disposition kinetics showing central (red) and peripheral (black) compartment concentrations for $p=1$ (Eqs. 38–41, panel (A)), $p=2$ (Eqs. 42–47, panel (B)), $p=3$ (Eqs. 48–55, panels (C) and (D)). Model parameters are shown in each panel. The symbol \blacktriangle denotes termination of all absorption stages.

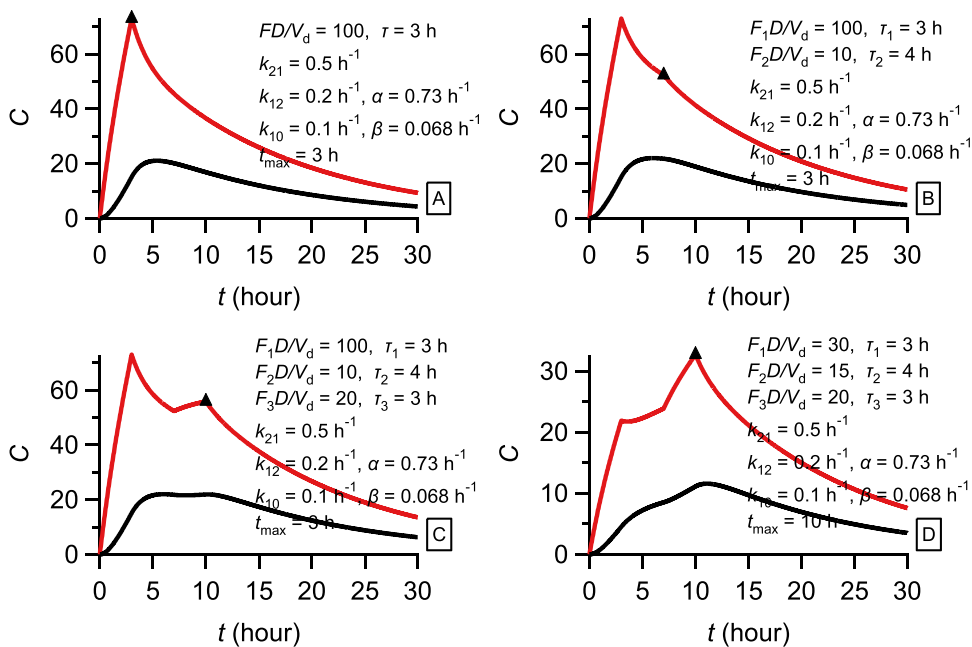
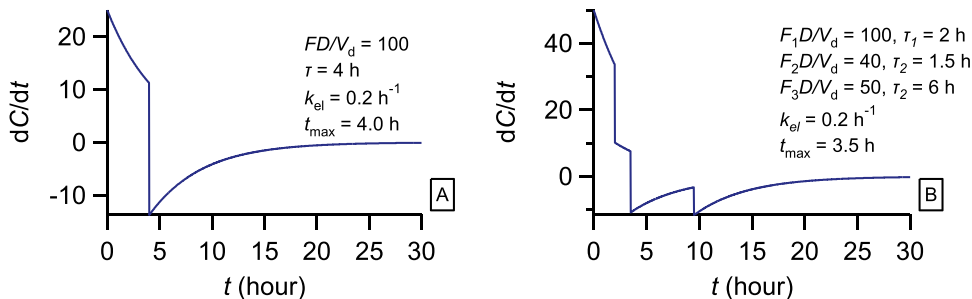


Fig. 5 Plots of the derivative dC/dt as a function of time. (A) $t_{max}=\tau=4.0$ h and the derivative was calculated from Eqs. 29 and 30. (B) $t_{max}=3.5$ h $<$ $\tau=9.5$ h and the derivative was calculated from Eqs. 34–37.



the generated curves, which poorly reflect the changes of the drug concentration in the central compartment $C(t)$, Fig. 4.

In all above plots the $(C(\tau), \tau)$ pair is a discontinuity datum point. When $t_{\max} = \tau$, there is a more patent change of the concentration–time curve in the neighborhood of the discontinuity time point, Figs. 3A, B, 4A, D. On the contrary, when $t_{\max} < \tau$, the discontinuity datum point lies in the descending part of the concentration–time curve, Figs. 3C, D, 4B, C and therefore this change is less abrupt. In Fig. 5, one can see the change of the derivative dC/dt for two examples with $t_{\max} = \tau$ and $t_{\max} < \tau$. In the former case, the derivative changes from positive to negative values at $t_{\max} = \tau$; in the latter case, the sign of the derivative is maintained negative close to τ and throughout the descending portion of the curve. These plots demonstrate that under experimental conditions the estimation of τ will be easier when $t_{\max} = \tau$. When $t_{\max} < \tau$, the presence of experimental error and the sparse sampling close to τ can make the estimation of τ impossible.

Model Fittings

In our previous work we analyzed experimental data of drugs (5, 7) exhibiting a single zero-order input. Here, we present only a similar example (paracetamol) and extend our applications to drugs belonging to various biopharmaceutical classes exhibiting more complex absorption and following one or two compartment model disposition. In all cases, modified release formulations were not examined.

i) Paracetamol. It is considered a high solubility compound with $>85\%$ absorption (11). We analyzed the experimental data of a pharmacokinetic study (12). The best fit results using Eqs. 29, 30 which adhere to the simplest model with a constant input rate and first-order elimination are shown in Fig. 6. According to the results presented in Fig. 6, paracetamol absorption is very fast and

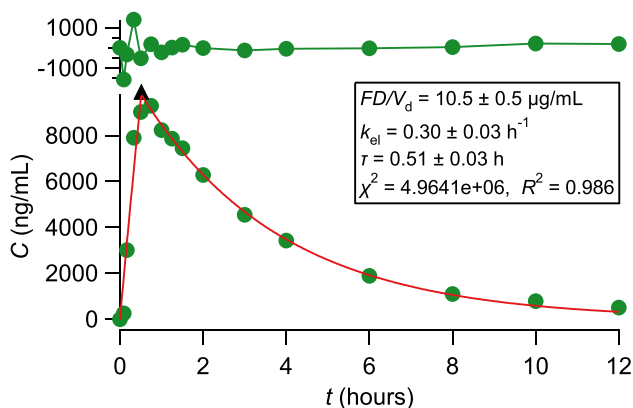


Fig. 6 Best fit results of Eqs. 29, 30 to paracetamol experimental data (12). The symbol \blacktriangle denotes the end of the absorption process. The top panel depicts the fit residuals.

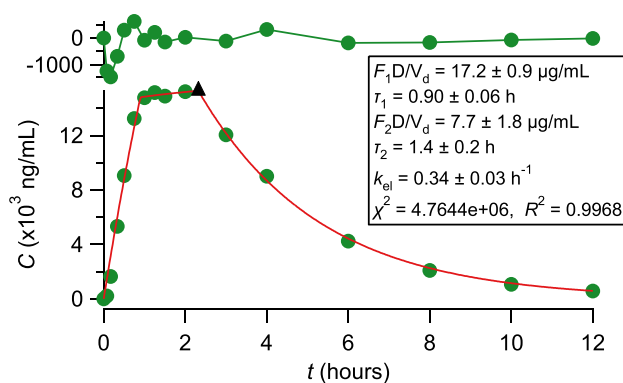


Fig. 7 Best fit results of Eqs. 31–33 to ibuprofen experimental data (12). The symbol \blacktriangle denotes the end of the absorption processes.

terminates at 0.51 ± 0.03 h. For comparative purposes the best fit results using Eq. 1 are shown in the supplementary material (Fig. S1).

- ii) Ibuprofen. This is a classical BCS class II drug with low solubility at pH 1.2 and 4.5 and high solubility at pH 6.8 since it is a carboxylic acid. We analyzed the experimental data of a pharmacokinetic study (12). The best fit results using Eqs. 31–33, which adhere to a model with two constant input rates and first-order elimination are shown in Fig. 7. These data reveal that absorption terminates at 2.3 h, namely, ibuprofen is absorbed in the small intestine. For comparative purposes the best fit results using Eq. 1 are shown in the supplementary material (Figs. S2–S3).
- iii) Almotriptan malate. This is a selective serotonin receptor agonist with hydrophilic properties. We analyzed the experimental data of a pharmacokinetic study (13). The best fit results using Eqs. 31–33, which adhere to a model with two constant input rates and first-order elimination are shown in Fig. 8. These data reveal that absorption terminates at 2.8 h, namely, almotriptan is absorbed in the small intestine. For comparative pur-

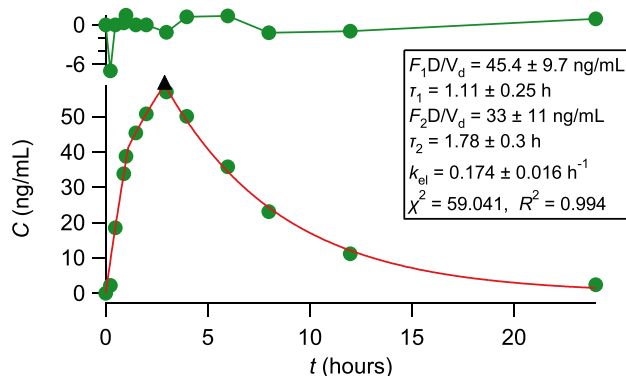


Fig. 8 Best fit results of Eqs. 31–33 to almotriptan experimental data (13). The symbol \blacktriangle denotes the end of the absorption processes.

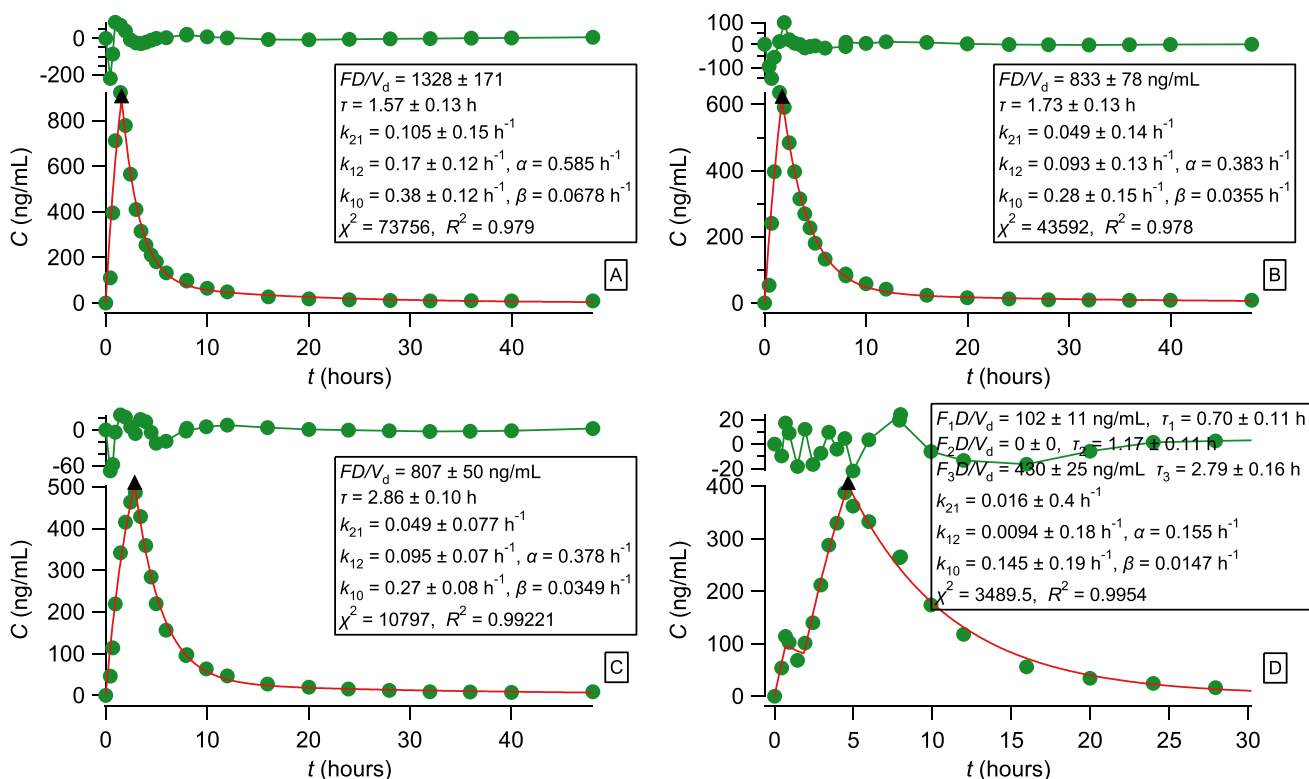


Fig. 9 Best fit results of Eqs. 29, 30 to test formulation under fasted (A), fed (B) conditions and reference formulation under fasted (C) conditions (15). Best fit results of Eqs. 48–55 to reference formulation under fed (D) conditions. The symbol ▲ denotes the end of the absorption processes.

poses the best fit results using Eq. 1 are shown in the supplementary material (Figs. S4–S5).

- iv) Cyclosporine. This is a Class II drug with very low solubility (14). We analyzed the experimental data of the fundamental bioequivalence study under fast and fed conditions, which led to the replacement of the reference formulation (Sandimmune) with the test formulation (Sandimmune Neoral) (15). The best fit results for the test (administered as a single oral dose of 180 mg) and reference (administered as a single oral dose of 300 mg) formulations under fasted and fed conditions are shown in Fig. 9.

The plots of Fig. 9 A, B and C reveal that the absorption of cyclosporine for the test formulation (Sandimmune Neoral) under both fasted and fed conditions as well as for the reference formulation (Sandimmune) under fasted conditions is described by a zero-order input process, which terminates at 1.6, 1.7, and 2.9 h, respectively. This shows that cyclosporine absorption terminates sooner with the test formulation than with the reference formulation. The graph in Fig. 9D shows the complex absorption of cyclosporine from the test formulation under fed conditions; in fact, the best fit corresponds to a model with three successive fluctuating input rates of total duration of 4.6 h. All these results are

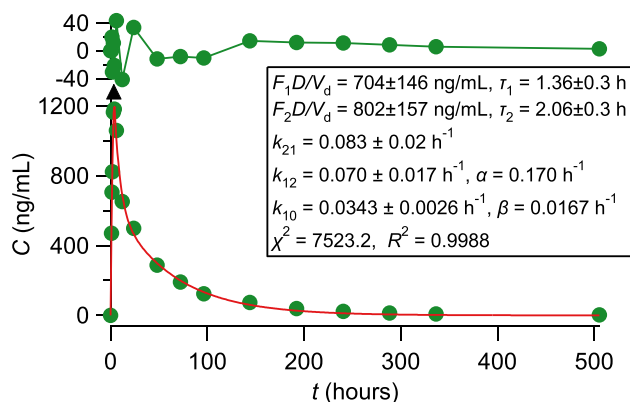


Fig. 10 Best fit results of Eqs. 42–48 to experimental data of nira-parib (16). The symbol ▲ denotes the end of the absorption processes.

indicative of the erratic absorption of cyclosporine from the reference formulation in presence of food. These findings are related to the hydrophobic nature of cyclosporine and the pharmaceutical differences of the two formulations, namely, the test formulation is a micro-emulsion while the reference formulation is a solution of cyclosporine in olive oil. The reader should also notice the high uncertainty (SDs) of the disposition parameters of cyclosporine in the panel of Fig. 9D in contrast to the

corresponding values in panels of Fig. 9 A, B and C. In all cases, the fits presented in Fig. 9 were superior (data not shown) to the fits of Eqs. 1 or 57 to the experimental data.

- v) Niraparib. This is an orally bioavailable anticancer agent. Here, we analyze the pharmacokinetics of an absolute bioavailability study of niraparib (16) using PBFTP models. The best fit results using Eqs. 42–48, which adhere to a model with two constant input rates

and two-compartment disposition are shown in Fig. 10. These data reveal that absorption terminates at 3.4 h, namely, niraparib is absorbed in the small intestine; the long stay of the drug in the body is due to the slow disposition characteristics. For comparative purposes the best fit results using Eqs. 1 and 57 (describing the drug concentration in the central compartment of a two-compartment model) without time restriction is presented in the supplementary data (Figs. S6-S7).

$$C(t) = \frac{FD}{V_d} \left[\frac{k_{21} - \alpha}{(k_a - \alpha)(\beta - \alpha)} e^{-\alpha t} + \frac{k_{21} - \beta}{(k_a - \beta)(\alpha - \beta)} e^{-\beta t} + \frac{k_{21} - k_a}{(\alpha - k_a)(\beta - k_a)} e^{-k_a t} \right] \quad (57)$$

Discussion

The analysis of data, Figs. 6, 7, 8, 9, 10, underlines the fact that the duration, τ , of the absorption process is a fundamental biopharmaceutical parameter of drug when administered as an immediate release formulation. The type of immediate release formulation can also have an impact on the τ estimate (see cyclosporine results, Fig. 9).

For years and years, the absorption rate constant became the sole parameter for expressing quantitatively the rate of drug absorption in classical and population pharmacokinetic studies. However, it was found to be the most variable parameter with non-meaningful physiological units (time^{-1}), not allowing a valid interspecies or pediatric scaling and relying on the unphysical assumption of infinite time of

absorption (17). The results presented in Figs. 6, 7, 8, 9, 10, if contrasted with the results derived from the fitting of Eqs. 1 and 57 to the same data presented in the supplementary material, clearly demonstrate the superiority of PBFTP models for the description of absorption characteristics of drugs/formulations. Roughly, the more complex the absorption is the better is the performance of PBFTP models compared to the Bateman equation (Eq. 1).

The assessment of permeation in the physiologically based pharmacokinetic (PBPK) models (10, 11) is based on permeability estimates; thus, the use of absorption rate constant for the assessment of the drug's input rate has been abandoned in the PBPK modeling work. The current work relies on the FAT concept (5, 7) and allows the estimation of τ , which can characterize each drug/formulation

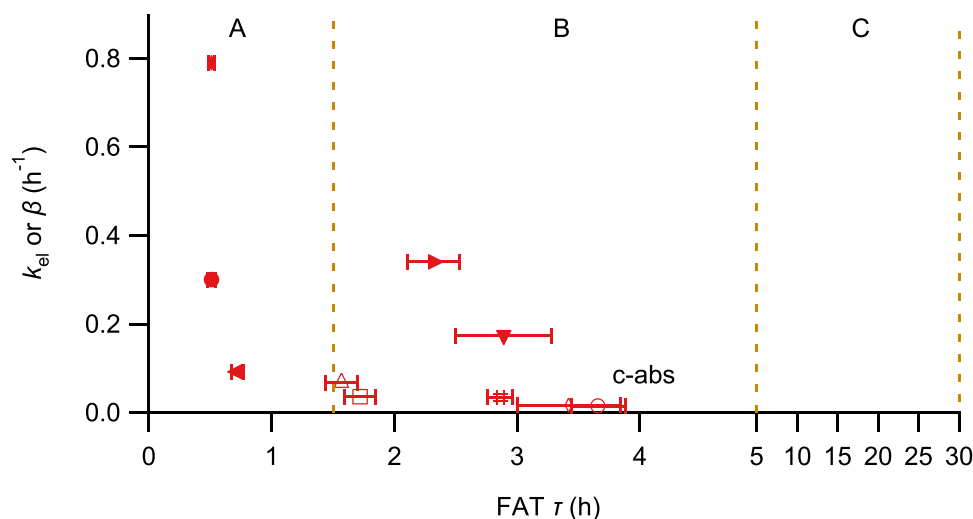


Fig. 11 Plot of elimination rate constant, k_{el} or β , estimates vs. finite absorption time (FAT), τ , estimates (\pm SD) Key: paracetamol (●), cyclosporine (Sandimmune Neoral, fasted) (Δ), ibuprofen (\blacktriangleright), almotriptan (\blacktriangledown), cyclosporine (Sandimmune Neoral fed) (\square), cyclosporine (Sandimmune, fasted) ($\#$), niraparib (\diamond), theophylline (5) (\blacktriangleleft), BMS-626529 drug (5, 18) (\blacklozenge). Filled symbols correspond to k_{el} estimates (one-compartment model drugs), while empty symbols correspond to β estimates (two-compartment model drugs). The term c-abs next to cyclosporine (Sandimmune, fed) (o) administered under fed conditions, denotes complex absorption.

given as an immediate release formulation, Figs. 6, 7, 8, 9, 10. This is so since τ is conceptually associated with the fundamental biopharmaceutical properties solubility and permeability as shown in Ref. (7). Intuitively, drugs/immediate release formulations can be classified into: i) rapidly absorbing $\tau < 1.5$ h like paracetamol and borderline cyclosporine (Sandimmune Neoral) administered under fasted conditions in the present study; ii) medium absorbing $1.5 \leq \tau < 5$ h like ibuprofen, almotriptan, cyclosporine (Sandimmune Neoral) administered under fed conditions as well as cyclosporine (Sandimmune) administered under fasted conditions in the present study and niraparib; iii) slow absorbing $5 \leq \tau < 30$ h not observed in the present study. For the first two categories, drug absorption takes place only in the small intestine, while for the third category, colon absorption is also operating. Several drugs/formulations exhibiting either selective regional permeability or solubility/ionization characteristics which lead to precipitation/re-dissolution comprise a fourth category characterized by a complex absorption profile like cyclosporine (Sandimmune) administered under fed conditions in the present study (see Fig. 9D). Figure 11 shows the proposed three categories (A, B and C) where a drug exhibiting complex absorption, denoted with c-abs, can also be classified in accord with its τ estimate. All estimates for τ are coupled with the corresponding estimate for drug's elimination rate constant k_{el} or β for drugs obeying one- or two-compartment model kinetics, respectively, Fig. 11.

Visual inspection of Fig. 11 reveals that the one-compartment model drugs paracetamol (Fig. 6) and theophylline (5), which are biowaivers, are located in Class A close to the ordinate. This is in accord with their extensive absorption calculated from oral data, if one applies the one-compartment model methodology described for theophylline in Ref. (5). This also applies for the BMS-626529 drug (5, 18). All cyclosporine formulations, ibuprofen and almotriptan are classified in Class B. Finally, it will be interesting to explore the classification presented in Fig. 11 in relation to other biopharmaceutical classifications (19–24).

In all examples analyzed the estimate for τ was found to be equal to t_{max} . Reliable estimates were derived for τ using our PBFTP software, Figs. 6, 7, 8, 9, 10, since an adequate number of samples were available throughout the time course of drug in the body. For the one-compartment model drugs exhibiting one input rate like paracetamol, this finding, $\tau = t_{max}$, is a logical consequence of the FAT concept. On the contrary, estimates for τ were not found in the descending leg of the curves ($\tau > t_{max}$), which could be observed in other drugs. Although this is theoretically possible (Fig. 5B), the fitting results and the statistical measures presented in Figs. 5, 6, 7, 8, 9, 10 provide conclusive evidence that $\tau = t_{max}$. However, the sampling design in the

neighborhood of τ and the magnitude of the experimental error of the data can make the estimation of τ not possible using the PBFTP software developed. Interested readers can contact the authors in case they wish to use it.

Overall, the application of finite absorption time (FAT) concept (5, 7) can open new avenues in the oral drug absorption research. Thus, the FAT concept can be also applied to interspecies and pediatric scaling using the τ estimates for each one of the species or children/adult as a core parameter in the scaling exercise. Additionally, the application of PBFTP software for re-analysis of oral data can provide input rate estimate(s) ($FD/\tau V_d$) which will be certainly associated with the rate controlling parameter(s) of absorption, solubility and/or permeability as explained in Ref. (7). Analysis of big oral data using machine learning techniques coupled with molecular descriptors can also elucidate critical factors of oral drug absorption phenomena. Besides, further applications of PBFTP models to the following topics can be envisaged too: i) development of models based on multiple oral drug administration; ii) construction of percent absorbed *versus* time plots and use in *in vitro-in vivo* correlations (IVIVC) under the prism of FAT concept; iii) extension/application of the modeling work to population studies; iv) coupling the PBFTP modes with pharmacodynamic models. These applications (i-iv) can be also considered in the light of non-linear (Michaelis–Menten) kinetics. All above, if coupled with the implications of finite absorption time models on bioavailability/bioequivalence issues (5, 25), point to a new era in the scientific and regulatory aspects of oral drug absorption. To this end, a Finite Time of Absorption-Group (FTA-G) has been established for all those interested in the experimental and theoretical analysis of oral drug absorption phenomena using the FTA concepts, which can be contacted via the website <http://www.athenarc.gr/>.

Conclusions

The finite absorption time (FAT) of drugs is a physiologically sound concept and the relevant estimate for τ derived from the analysis of oral data using an immediate release formulation is a characteristic drug property. The application of PBFTP models to the analysis of oral drug absorption data will enhance our understanding of oral drug absorption phenomena.

Supplementary Information The online version contains supplementary material available at <https://doi.org/10.1007/s11095-022-03230-0>.

Acknowledgments and Disclosures Panos Macheras will use this paper as a plea for the minister of education of Greece to allow emeriti professors supervise undergraduates, MSc and PhD students after obligatory

retirement. P.M. dedicates this work to his grandchildren Panos and Amelia (and all children of the world) since they always remind him to stay curious about everything. The authors thank the anonymous reviewers for their constructive comments.

Funding Statement There was no funding.

Declarations

Conflict of Interest Statement The authors declare no competing interests.

References

- Dost HF. *Der Blutspiegel. Kinetik der Konzentrationsabläufe in der Kreislaufflüssigkeit*. Leipzig: Thieme; 1953.
- Lovering EG, McGilveray IJ, McMillan I, Tostowaryk W. Comparative Bioavailabilities from Truncated Blood Level Curves. *J Pharm Sci*. 1975;64:1521–4. <https://doi.org/10.1002/jps.2600640921>.
- Sugano K. *Biopharmaceutics Modeling and Simulations: Theory, Practice, Methods, and Applications*. Wiley; 2012.
- Sugano K. Lost in modelling and simulation? *ADMET DMPK*. 2021;9:75–109. <https://doi.org/10.5599/admet.923>.
- Chryssafidis P, Tsekouras AA, Macheras P. Revising pharmacokinetics of oral drug absorption: II bioavailability-bioequivalence considerations. *Pharm Res*. 2021;38:1345–56. <https://doi.org/10.1007/s11095-021-03078-w>.
- Iranpour P, Lall C, Houshyar R, Helmy M, Yang A, Choi JI, Ward G, Goodwin SC. Altered Doppler flow patterns in cirrhosis patients: an overview. *Ultrasonography*. 2016;35:3–12. <https://doi.org/10.14366/ug.15020>.
- Macheras P, Chryssafidis P. Revising Pharmacokinetics of Oral Drug Absorption: I Models Based on Biopharmaceutical/Physiological and Finite Absorption Time Concepts. *Pharm Res*. 2020;37:187. <https://doi.org/10.1007/s11095-020-02894-w> (Erratum. *Pharm Res* 2020,37:206. <https://doi.org/10.1007/s11095-020-02935-4>).
- Abuhelwa A, Foster DJR, Upton RN. A Quantitative Review and Meta-models of the Variability and Factors Affecting Oral Drug Absorption-Part II: Gastrointestinal Transit Time. *AAPS J*. 2016;18:1322–33. <https://doi.org/10.1208/s12248-016-9953-7>.
- Sjögren E, Westergren J, Grant I, Hanisch G, Lindfors L, Lennernäs H, Abrahamsson B, Tannergren C. In silico predictions of gastrointestinal drug absorption in pharmaceutical product development: application of the mechanistic absorption model GI-Sim. *Eur J Pharm Sci*. 2013;49:679–98. <https://doi.org/10.1016/j.ejps.2013.05.019>.
- Sager JE, Yu J, Ragueneau-Majlessi I, Isoherranen N. Physiologically based pharmacokinetic (PBPK) modeling and simulation approaches: A systematic review of published models, applications, and model verification. *Drug Metab Dispos*. 2015;43:1823–37. <https://doi.org/10.1124/dmd.115.065920>.
- Paracetamol oral use, immediate release formulations product-specific bioequivalence guidance (europa.eu).
- Atkinson HC, Stanescu I, Frampton C, Salem II, Beasleyr CPH, Robson R. Pharmacokinetics and Bioavailability of a Fixed-Dose Combination of Ibuprofen and Paracetamol after Intravenous and Oral Administration. *Clin Drug Investig*. 2015;35:625–32. <https://doi.org/10.1007/s40261-015-0320-8>.
- Jansat JM, Costa J, Salva P, Fernandez FJ, Martinez-Tobed A. Absolute bioavailability, pharmacokinetics, and urinary excretion of the novel antimigraine agent almotriptan in healthy male volunteers. *J Pharmacokin Pharmacodyn*. 2002;42:1303–10. <https://doi.org/10.1177/0091270002239359>.
- Ismailos G, Reppas C, Dressman J, Macheras P. Unusual solubility behaviour of cyclosporine A in aqueous media. *J Pharm Pharmacol*. 1991;43:287–9. <https://doi.org/10.1111/j.2042-7158.1991.tb06688.x>.
- Mueller EA, Kovarik JM, van Bree JB, Grevel J, Lucker PW, Kutz K. Influence of a fat-rich meal on the pharmacokinetics of a new oral formulation of cyclosporine in a crossover comparison with the market formulation. *Pharm Res*. 1994;11:151–5. <https://doi.org/10.1023/a:1018922517162>.
- van Anandel L, Rosing H, Zhang Z, Hughes L, Kansra V, Sanghvi M, Tibben MM, Gebretensae A, Schellens JHM, Beijnen JH. Determination of the absolute oral bioavailability of niraparib by simultaneous administration of a ¹⁴C-microtracer and therapeutic dose in cancer patients. *Cancer Chemother Pharmacol*. 2018;81:39–46. <https://doi.org/10.1007/s00280-017-3455-x>.
- Macheras P. On an unphysical hypothesis of Bateman equation and its implications for pharmacokinetics. *Pharm Res*. 2019;36:94. <https://doi.org/10.1007/s11095-019-2633-4>.
- Brown J, Chien C, Timmins P, Dennis A, Doll W, Sandefer E, Page R, Nettles RE, Zhu L, Grasela D. Compartmental absorption modeling and site of absorption studies to determine feasibility of an extended-release formulation of an hiv-1 attachment inhibitor phosphate ester prodrug. *J Pharm Sci*. 2013;102:1742–51. <https://doi.org/10.1002/jps.23476>.
- Amidon GL, Lennernäs H, Shah VP, Crison JR. A Theoretical basis for a biopharmaceutic drug classification: The correlation of in vitro drug product dissolution and in vivo bioavailability. *Pharm Res*. 1995;12:413–20. <https://doi.org/10.1023/A:1016212804288>.
- Wu CY, Benet LZ. Predicting drug disposition via application of BCS: transport/absorption/ elimination interplay and development of a biopharmaceutics drug disposition classification system. *Pharm Res*. 2005;22:11–23. <https://doi.org/10.1007/s11095-004-9004-4>.
- Macheras P, Karalis V. A non-binary biopharmaceutic classification of drugs: the ABΓ system. *Int J Pharm*. 2014;464:85–90. <https://doi.org/10.1016/j.ijpharm.2014.01.022>.
- Rinaki E, Valsami G, Macheras P. Quantitative biopharmaceutics classification system (QBCS): The central role of dose/solubility ratio. *Pharm Res*. 2003;20:1917–25. <https://doi.org/10.1023/B:PHAM.000008037.57884.11>.
- Charkoftaki G, Dokoumetzidis A, Valsami G, Macheras P. Elucidating the role of dose in the biopharmaceutics classification of drugs: The concepts of critical dose, effective in vivo solubility, and dose-dependent BCS. *Pharm Res*. 2012;29:3188–98. <https://doi.org/10.1007/s11095-012-0815-4>.
- Macheras P, Iliadis A, Melagraki G. A reaction-limited in vivo dissolution model for the study of drug absorption: Towards a new paradigm for the biopharmaceutic classification of drugs. *Eur J Pharm Sci*. 2018;117:98–106. <https://doi.org/10.1016/j.ejps.2018.02.003>.
- Tsekouras AA, Macheras P. Re-examining digoxin bioavailability after half a century: Time for changes in the bioavailability concepts. *Pharm Res*. 2021;38:1635–8. <https://doi.org/10.1007/s11095-021-03121-w>.

Publisher's Note Springer Nature remains neutral with regard to jurisdictional claims in published maps and institutional affiliations.